Proceedings of the Twenty-seventh (2017) International Ocean and Polar Engineering Conference **www.isope.org**
San Francisco, CA, USA, June 25-30, 2017

ISBN 978-1-880653-97-5; ISSN 1098-6189

MPS Simulation of Sloshing Flows in a Tuned Liquid Damper

*Xiao Wen, Xiang Chen, Decheng Wan**
Collaborative Innovation Center for Advanced Ship and Deep-Sea Exploration, State Key Laboratory of Ocean Engineering, School of Naval Architecture, Ocean and Civil Engineering, Shanghai Jiao Tong University, Shanghai, China
*Corresponding author

ABSTRACT

In the present paper, our in-house meshless solver MLParticle-SJTU, based on the improved MPS (moving particle semi-implicit) method, is employed to simulate the liquid sloshing in the tuned liquid damper (TLD). For the validation purpose, parameters from experiments in previous literature are adopted in first numerical simulation, the roll angle and wave shapes inside the TLD show agreement with the experimental data. Then, the influence of various external excitation on the damping characteristic of TLD has been studied through the changing of motion amplitude and frequency of a sliding mass. The numerical results indicate that the damping characteristic is more distinct when the excitation frequency falls near the natural frequency of the TLD system, and the flow in the TLD turns from traveling wave into the quasi-dam-break flow when the excitation amplitude increases from 50 mm to 200 mm.

KEY WORDS: Particle method; MPS (moving particle semi-implicit); MLParticle–SJTU solver; TLD (tuned liquid damper); sloshing; roll.

INTRODUCTION

In this paper, the sloshing phenomenon in a tuned liquid damper (TLD), which is mainly composed of rectangular tank with the freedom of roll motion, is numerically studied. In the ship engineering, the TLD is commonly employed as the anti-roll device to suppress the roll motion of ship operating in severe sea. Compared with active ship stabilizer, the TLD have advantages of simple structure, low cost and easy maintenance, so a lot of attention has been paid to both experimental (Vera et al., 2010) and numerical researches on the sloshing in TLD (Bulian et al., 2010).

The damping characteristic of TLD mainly depends on the sloshing in the tank and the properties of liquid in it. The physical behavior of sloshing flow in the partially filled TLD is similar to shallow water waves (Verhagen and Van, 1965), and shows high non-linear when violent sloshing occurs. Due to the phase lag between the roll motion and the wave movement, the roll motion of tank is damped by the moment induced by the impact loads of waves acting on inner wall of tank.

One of the oldest papers concerned with experimental examination of fluid dynamics in a moving container is probably that by Housner (1963). Souto et al. (2011) design a series of experiments to study the sloshing characteristics of different fluid in a free-surface tank. However, only the local flow field information can be obtained from experiments. To acquire the global information, we need turn to Computational Fluid Dynamics (CFD). In recent years, with the ongoing development of CFD, many numerical methods have been applied to the sloshing phenomenon in TLD. Van (2001) simulated the problems of water sloshing in free-surface and U-tube anti-roll tanks with VOF method, and obtained results which are in good agreement with experimental study, including the water height, the sway force and roll-moment amplitudes and phases. Bulian and Souto (2010) used SPH method to treat the coupling problems same as the one in this paper, and gained the motion response of the TLD in resonance region and off-resonance region. However, few researches are conducted with the moving particle semi-implicit (MPS) method, which can handle the steep deformation of the free surface well and provide high precision and good stability in solving such a sloshing problem.

This paper focuses on the simulations of the sloshing phenomenon with the moving particle semi-implicit (MPS) method (Koshizuka and Oka, 1996), which is a Lagrangian meshless method for incompressible flows with a free surface, is distinguished from SPH method that the pressure field is obtained by solving a Poisson pressure equation at every step (Cummins and Rudman, 1999). Therefore, an explicit geometric compatibility between the mass and the volume can be achieved. Besides, the incompressible treatment allows a second semi-implicit amendment of velocity field, which can significantly improve the stability of numerical simulation. As so far, the MPS method has proven to be valid in liquid sloshing, water-entry flow, dam break flow, fluid-structure interaction and so on. Lee et al. (2011) improved the accuracy and efficiency of MPS method by using optimal source term, optimal gradient and collision models, and improved solid-boundary treatment and search of free-surface particles. Hwang et al. (2016) successfully applied MPS method to the simulation of sloshing flow interacting with elastic baffles by proposing a new scheme, corresponding to fluid–structure coupling force. The major drawback of

MPS is that the pressure of free surface must be explicitly set to zero at every step. However, the problem has been alleviated because a lot of numerical nice work have been carried out to enhance the ability of the MPS method (Kondo and Koshizuka, 2011; Zhang and Wan, 2012).

NUMERICAL SCHEME

Governing Equations

The governing equations in the MPS method include the mass and momentum conservation equations:

$$\frac{1}{\rho}\frac{D\rho}{Dt} = -\nabla \cdot \boldsymbol{V} = 0 \tag{1}$$

$$\frac{D\boldsymbol{V}}{Dt} = -\frac{1}{\rho}\nabla P + \nu\nabla \boldsymbol{V} + \boldsymbol{g} \tag{2}$$

where ρ denotes the density, P is the pressure, V is the velocity, g is the gravity acceleration, ν the kinematics viscosity and t is the flow time.

Particle Interaction Models

In the present work, we adopt the following modified kernel function suggested by Zhang and Wan (2012):

$$W(r) = \begin{cases} \dfrac{r_e}{0.85r + 0.15r_e} - 1 & 0 \le r < r_e \\ 0 & r_e \le r \end{cases} \tag{3}$$

Where $r = |\, r_i - r_j \,|$ denotes the distance between two particles, r_e is the supported radius of the particle interaction domain.

To calculate the weighted average in MPS method, particle number density is defined as (Koshizuka et al., 1998):

$$< n >_i = \sum_{j \ne i} W(|\, \boldsymbol{r}_j - \boldsymbol{r}_i \,|) \tag{4}$$

Gradient Model

In this paper, the gradient operator can be discretized into a local weighted average of radial function as follow (Tanaka M. and Masunaga T, 2010):

$$< \nabla P >_i = \frac{D}{n^0}\sum_{j \ne i}\frac{P_j + P_i}{|\, \boldsymbol{r}_j - \boldsymbol{r}_i \,|^2}(\boldsymbol{r}_j - \boldsymbol{r}_i)\cdot W(|\, \boldsymbol{r}_j - \boldsymbol{r}_i \,|) \tag{5}$$

Where D is the number of space dimension, r represents coordinate vector of fluid particle, $W(r)$ is the kernel function and n^0 denotes the initial particle number density for incompressible flow.

Laplacian Model

Laplacian operator is derived by Koshizuka et al. (1998) from the physical concept of diffusion as:

$$< \nabla^2 \phi >_i = \frac{2D}{n^0 \lambda}\sum_{j \ne i}(\phi_j - \phi_i)\cdot W(|\, \boldsymbol{r}_j - \boldsymbol{r}_i \,|) \tag{6}$$

$$\lambda = \frac{\sum_{j \ne i} W(|\, \boldsymbol{r}_j - \boldsymbol{r}_i \,|)\cdot |\, \boldsymbol{r}_j - \boldsymbol{r}_i \,|^2}{\sum_{j \ne i} W(|\, \boldsymbol{r}_j - \boldsymbol{r}_i \,|)} \tag{7}$$

In Eq.6, the parameter λ is introduced to keep the increase of variance equal to analytical solution.

Model of Incompressibility

In the present work, we adopt a mixed source term for PPE which is proposed by Tanaka and Masunaga (2010), this improved PPE is rewritten by Lee et al. (2011) as:

$$< \nabla^2 P^{n+1} >_i = (1-\gamma)\frac{\rho}{\Delta t}\nabla \cdot V_i^* - \gamma\frac{\rho}{\Delta t^2}\frac{< n^* >_i - n^0}{n^0} \tag{8}$$

Where： γ is a blending parameter to account for the relative contributions of the two terms. The range of $0.01 \le \gamma \le 0.05$ is better according to numerical experiments conducted by Lee et al. (2011).

Free Surface Boundary Condition

In the MPS method, the kinematic condition is directly satisfied in Lagrangian particle method, while the dynamic condition is implemented by assigning zero pressure to the free surface particles. In traditional MPS method, particle satisfying (Koshizuka et al., 1998):

$$< n >_i^* < \beta \cdot n^0 \tag{9}$$

is considered as on the free surface, where β is 0.97 in this paper.

To improve the accuracy of surface particle detection, we adopt a new detection method in which a vector function is defined as follow (Zhang and Wan, 2011):

$$< \boldsymbol{F} >_i = \frac{D}{n^0}\sum_{j \ne i}\frac{1}{|\, \boldsymbol{r}_i - \boldsymbol{r}_j \,|}(\boldsymbol{r}_i - \boldsymbol{r}_j)W(\boldsymbol{r}_{ij}) \tag{10}$$

The vector function $\boldsymbol{F}$ represents the asymmetry of arrangements of neighbor particles. Thus, particles satisfying:

$$<|\, \boldsymbol{F} \,|>_i \; > \; \alpha \tag{11}$$

are considered as surface particle, where α is a parameter with a value of $0.9\,|F\,|^0$ in this paper, $|F\,|^0$ is the initial value of $|F\,|$ for surface particle.

Wall Boundary Condition

As shown in Fig. 1, the wall boundary condition is represented by three layer of wall particles. One layer of wall particles is set along the solid wall, and involved in the pressure calculation. In order to prevent the fluid particles near the solid wall from been misjudged as free surface particles, two layer of ghost particles are included inside the wall and only involved in the calculation of particle number density. In the

original MPS method, all the wall particles are unmovable, so the wall boundary condition is not flexible.

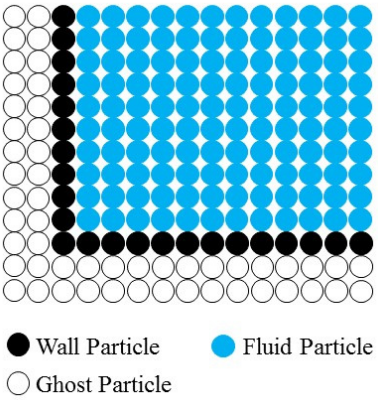

Fig. 1 Particles distribution near the wall

NUMERICAL SIMULATION

Simulation Model

The simulation model in this paper is based on the TLD device used by Souto (2010), displayed in Fig. 2. The device consists of two parts, i.e., a rectangular tank limited to roll motion and a horizontal linear guide fixed on the rotation center. Along the guide a sliding mass moves with a defined harmonic motion, to excite the roll of the tank.

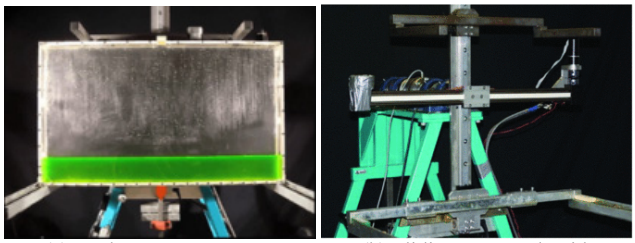

(a) Tank (b) Sliding mass and guide

Fig. 2 TLD testing device (Souto, 2010)

The width of the tank is much smaller than the length and height, that the physical model can transformed into a 2D rectangular tank in numerical simulation, as shown in Fig. 3. The size of the tank is 900 mm × 508 mm. The water depth is 92 mm, in order to keep the first sloshing frequency of water equal to the nature frequency of the TLD system. In the MPS method, the TLD system is substituted by uniformly distributed particles. The initial distance between particles is 4 mm. The total number of particles is 7584, including 5424 fluid particles and 2160 boundary particles.

The sliding mass is not included in the simulation model in the form of particles. Instead, an analytical model of the TLD system is introduced to incorporate the motion of the sliding mass into the MPS code. The analytical model is derived from the equation of moment of momentum of the tank, with the values of the parameters in the equation determined by a series of tests (Bulian et al., 2010). The analytical model is described as follow:

$$[I_0 + m]\xi_m^2(t)\cdot\ddot{\varphi} + 2m\xi_m(t)\dot{\xi}_m(t)\cdot\dot{\varphi} - g\cdot S_G\cdot\sin(\varphi) + m\cdot g\cdot\xi_m(t)\cdot\cos(\varphi) = Q_{damp}(t) + Q_{fluid}(t) \quad (12)$$

$$Q_{damp}(t) = -K_{df}\cdot sign(\dot{\varphi}) - B_{\varphi}\cdot\dot{\varphi} \quad (13)$$

Where, φ [rad] is the roll angle, $g = 9.81$ [m/s^2] is the gravitational acceleration, $I_0 = 26.9$ [kg · m^2] is the polar moment of inertia of the rigid system with respect to the rotation axis, $m = 4.978$ [kg] is the mass of the moving weight, $\xi_m(t)$ [m] is the instantaneous (imposed) position of the excitation weight along the linear guide (tank-fixed reference system), $\dot{\xi}_m(t)$ [m/s] and $\ddot{\xi}_m(t)$ [m/s^2] are the first and second time derivatives of $\xi_m(t)$ [m], $S_G = M_R\cdot\eta_G = -29.2$ [kg · m] is the static moment of the rigid system with respect to the rotation axis, M_R [kg] is the total mass of the rigid system, η_G [m] is the (signed) distance of the center of gravity of the rigid system with respect to the rotation axis (tank-fixed reference system), $Q_{damp}(t) = -K_{df}\cdot sign(\varphi) - B_{\varphi}\cdot\dot{\varphi}$ [N · m] is the assumed form of roll damping moment comprising:

A dry friction term — $K_{df}\cdot sign(\dot{\varphi})$ with $K_{df} = 0.540$ [N · m] being the dry friction coefficient

A linear damping term — $B_{\varphi}\cdot\dot{\varphi}$ with $B_{\varphi} = 0.326$ [N · m/(rad/s)] being the linear damping coefficient

When $\ddot{\varphi}_n$ is calculated at n^{th} time step according to Eq. 12, $\dot{\varphi}_{n+1}$ and φ_{n+1} can be get from the Eq. 14 and Eq. 15.

$$\dot{\varphi}_{n+1} = \dot{\varphi}_n + \ddot{\varphi}_n\cdot\Delta t \quad (14)$$

$$\varphi_{n+1} = \varphi_n + \dot{\varphi}_n\cdot\Delta t \quad (15)$$

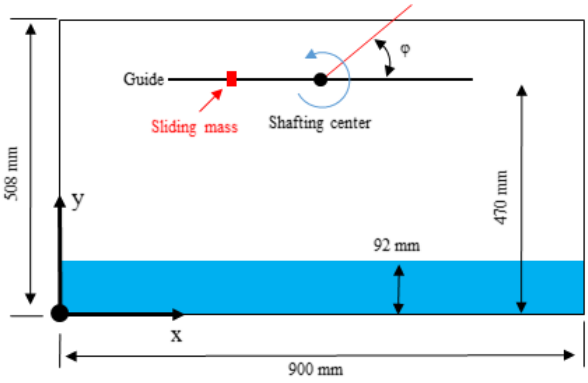

Fig. 3 Simulation model

Model Validation

In this part, numerical simulations under two different conditions are carried out, to test the feasibility of the improved MPS model when applied to solve TLD sloshing problem. One condition is A=100 mm, $\omega = \omega_0$, the other is A=150 mm, $\omega = 0.9\omega_0$, where A is the motion amplitude of the mass, ω is the motion frequency of the mass, and ω_0 is the natural frequency of the system. The A and ω also

represent excitation amplitude and frequency. With defined A and ω, the instantaneous positon $\xi_m(t)$ and the velocity $\dot{\xi}_m(t)$ of the sliding mass are obtained. However, the values of $\xi_m(t)$ and $\dot{\xi}_m(t)$ will not uniquely determined by A and ω in this section.

Different from numerical simulation, the motion of the sliding mass is technically difficult to be purely sinusoidal in real experiments. In fact, the motion curve is found to consist of four parabolic branches in every period. For better comparison between numerical simulation and experiments, $\xi_m(t)$ and $\dot{\xi}_m(t)$ are set to the values get from measurement in experiments.

Fig. 4 shows the motion response of empty tank in the condition of A=150 mm, $\omega = 0.9\omega_0$, corresponding to the off-resonance excitation. Nice beating phenomenon can be observed because the excitation frequency is very close to the natural frequency of the TLD system, and the curve obtained from numerical simulation match well with the curve from experiments, proving the validation of the MPS method. However, there are still some difference between numerical and experimental results over time, in both amplitude and phase. This is because the excitation amplitude and frequency in simulation is not absolutely consistent with experiments.

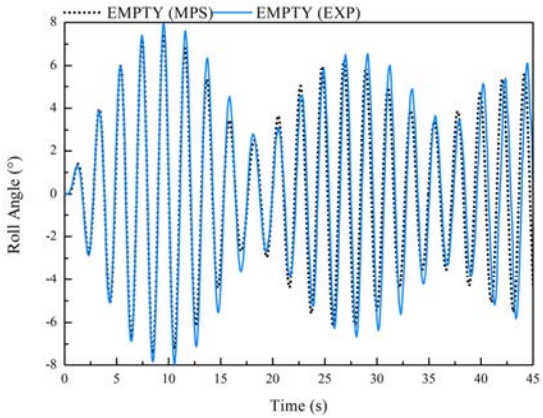

Fig. 4 Roll angle of empty tank, A=150 mm, $\omega = 0.9\omega_0$

In Fig. 5, due to the liquid damping inside the TLD tank, the beating phenomenon shows up only at the beginning of roll motion. Then, the roll motion is modulated to a constant amplitude oscillation, with an amplitude about 5 degrees, smaller than the peak amplitude of empty tank, about 8 degrees. This means that the damping characteristic of TLD can be captured by the MPS method. Similar to the roll angle of empty tank, there is some difference between numerical and experimental results, which is acceptable.

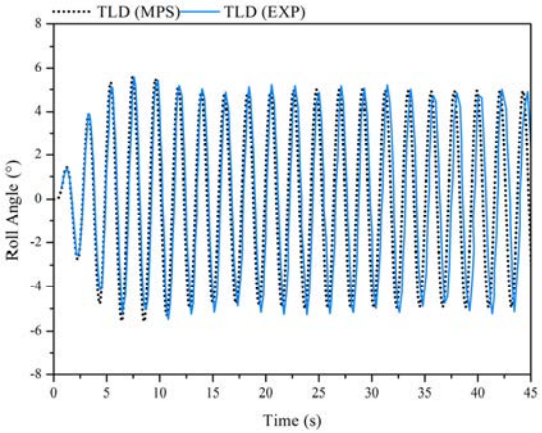

Fig. 5 Roll angle of TLD, A=150 mm, $\omega = 0.9\omega_0$

The two groups of pictures in Fig. 6 and Fig. 7 show the wave shapes in TLD tank at two different instants in the condition of A=100 mm, $\omega = 1.0\omega_0$, corresponding to resonance excitation. The breaking wave appears because larger motion amplitude oscillation can be induced by resonance excitation in this case, which has been found to be an important factor of damping characteristic of TLD (Bouscasse et al., 2014b). The instantaneous shapes of breaking wave reach a good agreement with the results gained from experiments and SPH method.

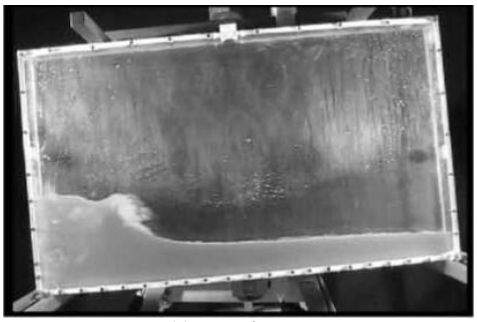

(a) Experiments

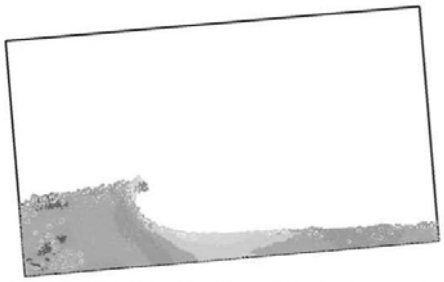

(b) SPH method

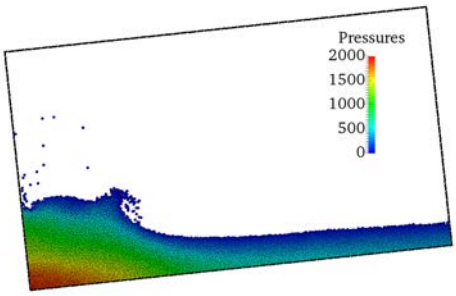

(c) MPS method

Fig. 6 Wave shapes, $t/T0 = 8.66$, A=100 mm, $\omega = 1.0\omega_0$

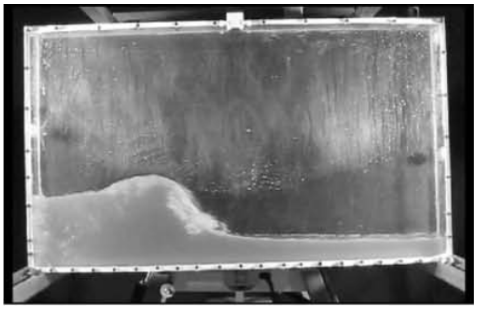

(a) Experiments

(b) SPH method

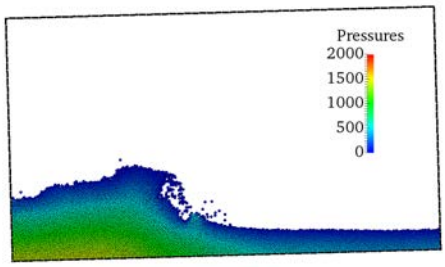

(c) MPS Method

Fig. 7 Wave shapes, $t/T0 = 8.85$, A=100 mm, $\omega = 1.0\omega_0$

Damping Characteristic of TLD

The roll motion of TLD in different conditions is simulated to study the damping characteristic of TLD. The sliding motion of the mass is determined as Eq. 16 and Eq. 17.

$$\xi_m(t) = -A \cdot \sin(\omega t) \tag{16}$$

$$\dot{\xi}_m(t) = -A \cdot \omega \cdot \cos(\omega t) \tag{17}$$

With a variety of motion amplitudes and frequencies of the sliding mass, different external excitations are imposed on the TLD system. Table 1 shows the test matrix of numerical simulation in this part. Seven motion frequencies ($\omega = 0.7\omega_0$, $\omega = 0.8\omega_0$, $\omega = 0.9\omega_0$, $\omega = 1.0\omega_0$, $\omega = 1.1\omega_0$, $\omega = 1.2\omega_0$, $\omega = 1.3\omega_0$) are respectively applied to four motion amplitudes (A=50 mm, A=100 mm, A=150 mm, A=200 mm), so there are total 28 cases been simulated in this part. The nature frequency ω_0 and the natural period T_0 of the present TLD system are equal to 3.26 rad/s and 1.925 s respectively.

Table 1. Test matrix

A / (ω/ω_0)	50 mm	100 mm	150 mm	200 mm
0.7	0.7/50	0.7/100	0.7/150	0.7/200
0.8	0.8/50	0.8/100	0.8/150	0.8/200
0.9	0.9/50	0.9/100	0.9/150	0.9/200
1.0	1.0/50	1.0/100	1.0/150	1.0/200
1.1	1.1/50	1.1/100	1.1/150	1.1/200
1.2	1.2/50	1.2/100	1.2/150	1.2/200
1.3	1.3/50	1.3/100	1.3/150	1.3/200

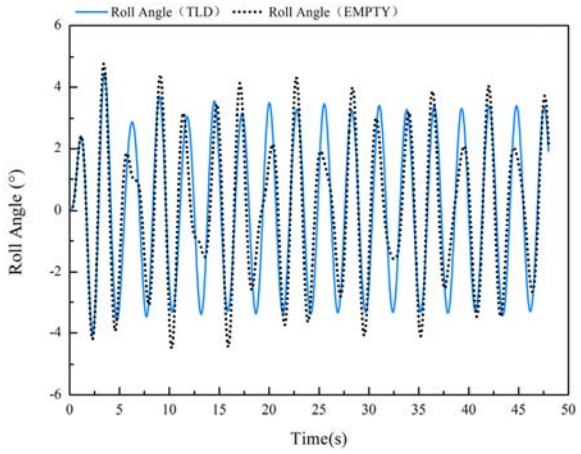

(a) $\omega = 0.7\omega_0$

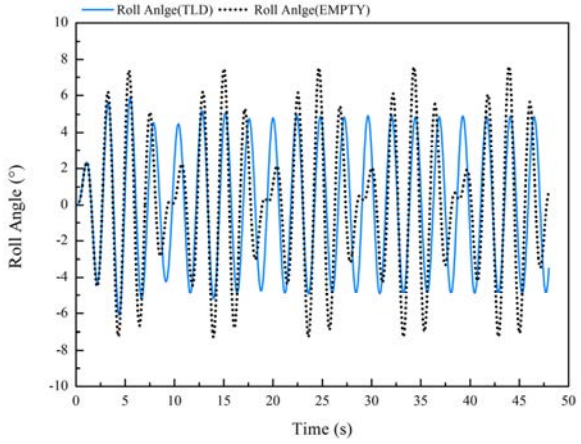

(b) $\omega = 0.8\omega_0$

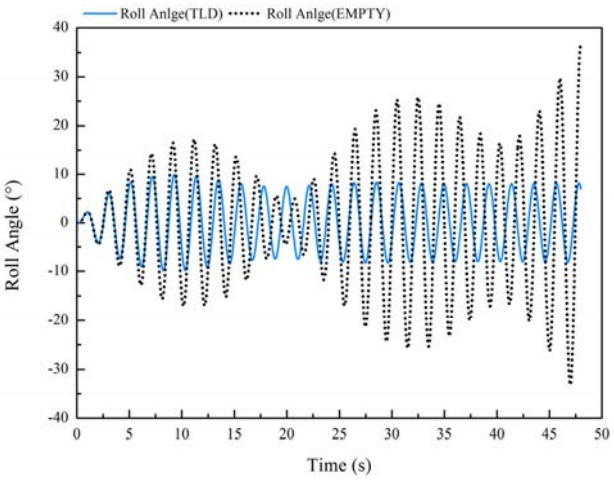

(c) $\omega = 0.9\omega_0$

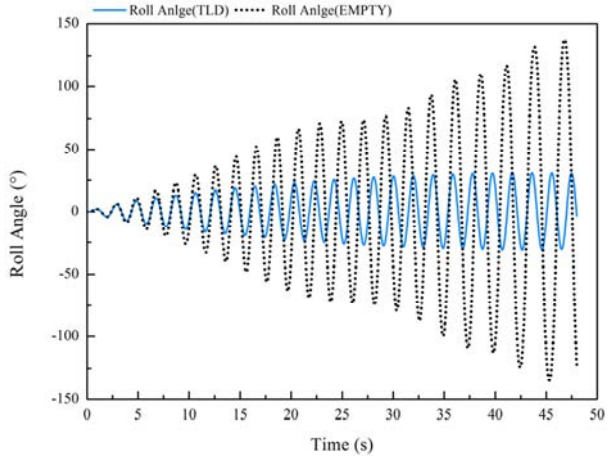

(d) $\omega = 1.0\omega_0$

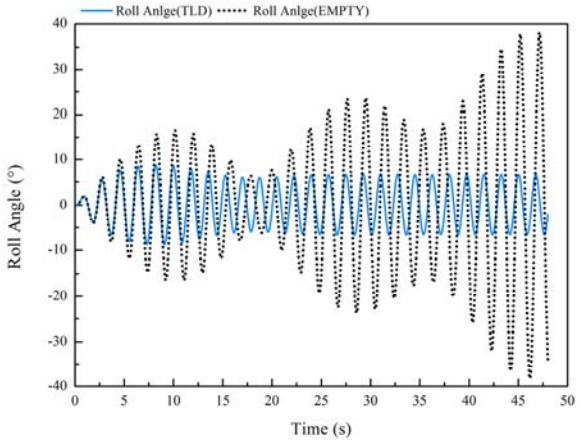

(e) $\omega = 1.1\omega_0$

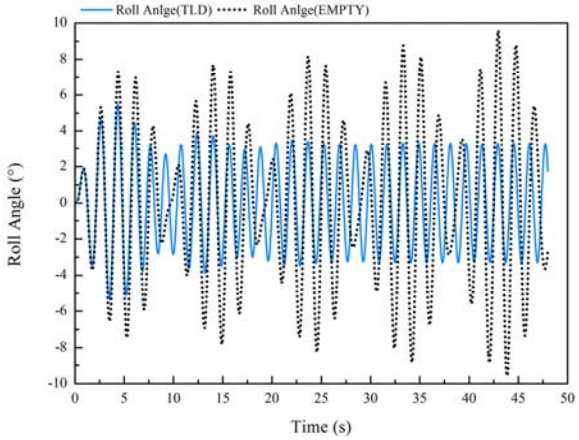

(f) $\omega = 1.2\omega_0$

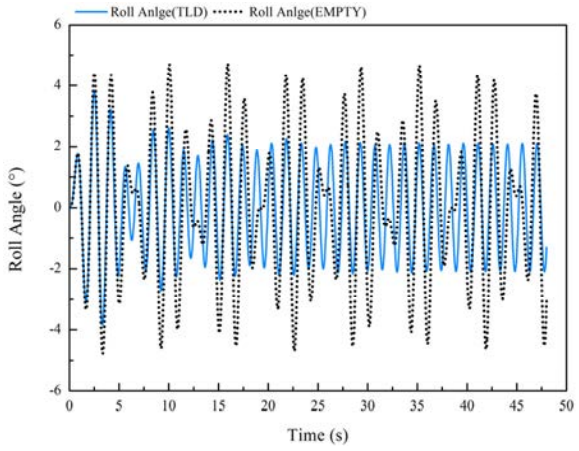

(g) $\omega = 1.3\omega_0$

Fig. 8 Roll angle of empty tank and TLD, A=150 mm

The response amplitude of empty tank increases with the excitation frequency getting closer to the natural frequency of the TLD system. In off-resonance region ($\omega \neq 1.0\omega_0$), The beating phenomenon appears, and the beat period gets longger near the naturel frequency. In resonance region ($\omega = 1.0\omega_0$), the response amplitude keeps increasing in a approximately linear law throughout the calculation time, and finally, the roll angle will exceed 180 degrees, which means the tank will be overturned.The damping characteristic of TLD is apparent under various external excitation frequency, with the roll motion of tank vastly suppressed. The tank is limited to a constant amplitude oscillation, in both resonance region and off-resonance region, and the constant oscillation is much smaller than the motion amplitude of empty tank under the same excitation.

Although TLD is a passive anti-roll device, its damping effect can be observed at the early stage of the motion, and its reaction time is short enough for practical application. In Fig. 8d, the response amplitude of TLD keep increasing in the beginning of roll motion in resonance region, but at a much smaller speed than that in empty tank. After 40 seconds, the amplitude become constant. In off-resonance region, the beating phenomenon disappears after the first beat period and the roll

motion rapidly turns into a constant amplitude oscillation.

The damping characteristic of TLD is stronger when the excitation frequency getting closer to the natural frequency of the TLD system. In order to characterize the size of the damping effect, one variable, amplitude reduction ratio, is defined. It is equal to the reduced percentage of maximum amplitude when the motion of empty tank turns to the constant amplitude oscillation of TLD. Fig. 9 shows the amplitude reduction ratio of TLD under different external excitations. In different excitation amplitudes, the same rule is discovered. With the excitation frequency below the natural frequency of TLD system, the damping characteristic is not distinct, even can be ignored in some cases. Along with the increase of the excitation frequency, the amplitude reduction ratio rapidly rises, and reaches to a peak in the resonance region. Then the damping characteristic of TLD gradually decreases if the excitation frequency keep increasing.

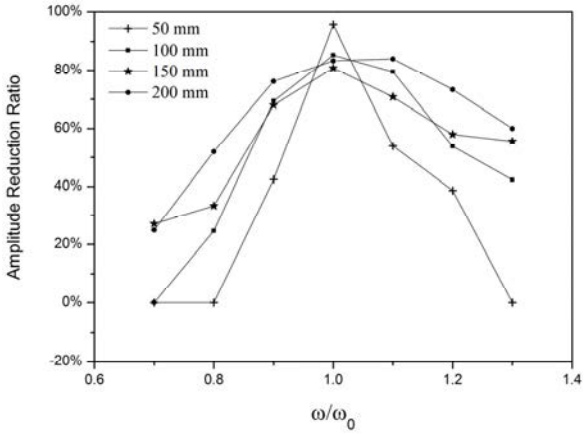

Fig. 9 Amplitude reduction ratio under different external excitations

Sloshing Wave in TLD

Bouscasse (2014a) pointed out that the breaking waves in TLD can significantly affect the damping characteristic. In Fig. 10, the sloshing wave shapes of TLD obtained by the MPS method are shown, which match well with the results of experiments. The four resonance cases are chosen because the sloshing wave shapes are most evident in resonance region. Two instants are selected for each case, one with the maximum angle and one with a flat angle.

In Fig. 10a, the sloshing waves train from one side of TLD tank to the other side, without breaking wave. In Fig. 10b, a plunge breaking event appears in the middle of the tank, and violent impact on the inner wall happens when the tank rolls to the maximum angle. In Fig. 10c and 10d, when the TLD rolls to the maximum angle, the water almost accumulates on one side of the tank, and the motion of water can be classified as a quasi-dam-break type flow.

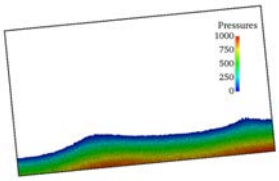

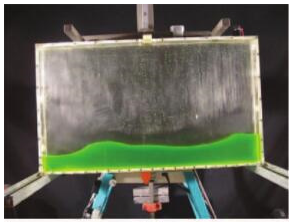

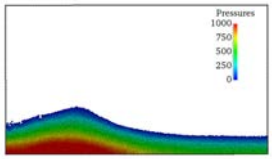

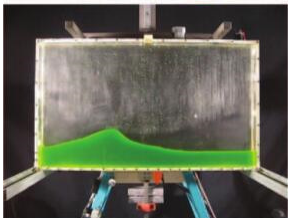

(a) A=50 mm, $\omega = 1.0\omega_0$

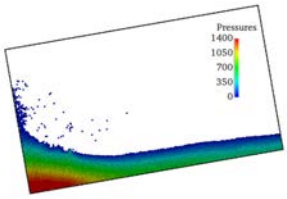

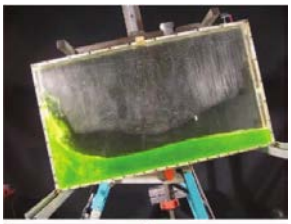

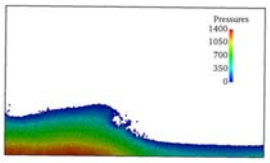

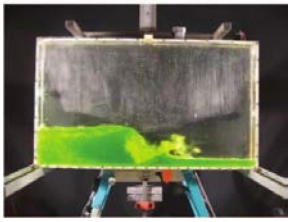

(b) A=100 mm, $\omega = 1.0\omega_0$

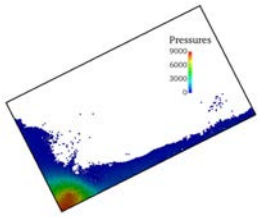

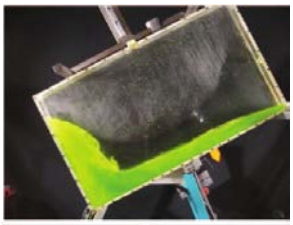

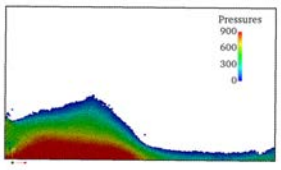

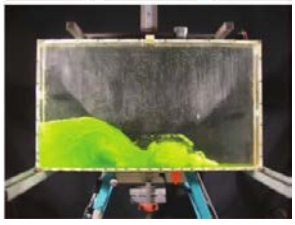

(c) A=150 mm, $\omega = 1.0\omega_0$

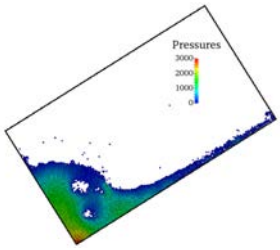

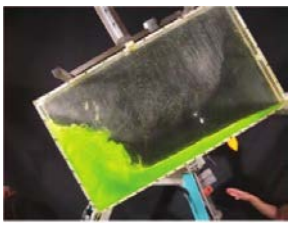

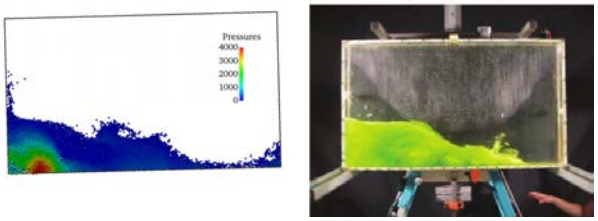

(d) A=200 mm, $\omega = 1.0\omega_0$

Fig. 10 Wave shapes in TLD, MPS (left), Experiments (right).

CONCLUSIONS

In this paper, the in-house solver MLParticle-SJTU is employed to study the liquid sloshing in TLD system. The solver is developed based on the improved MPS method and has been applied into numerous free surface flows in our previous works.

As a result of liquid sloshing, the TLD has excellent damping characteristic. The damping effect of TLD largely increases when the excitation amplitude getting closer to the natural frequency of the TLD system, and is strongest in the resonance cases, in which beyond 80% of the TLD oscillation is suppressed.

The damping characteristic belongs to a passive function, but can come into effect within a short time after the motion begins, which is important in practical application of TLD. With the excitation amplitude increasing from 50 mm to 200 mm, different kinds of sloshing flow can be observed in the TLD, at first, only a wave trains without breaking waves, then a plunging breaking event takes place, finally a quasi-dam-break flow occurs. From comparison with experiments and SPH method, it can been seen that the MPS method is fully capable of capturing the sloshing feature of TLD system.

ACKNOWLEDGEMENTS

This work is supported by the National Natural Science Foundation of China (51379125, 51490675, 11432009, 51579145), Chang Jiang Scholars Program (T2014099), Shanghai Excellent Academic Leaders Program (17XD1402300), Shanghai Key Laboratory of Marine Engineering (K2015-11), Program for Professor of Special Appointment (Eastern Scholar) at Shanghai Institutions of Higher Learning (2013022), Innovative Special Project of Numerical Tank of Ministry of Industry and Information Technology of China(2016-23/09) and Lloyd's Register Foundation for doctoral student, to which the authors are most grateful.

REFERENCES

Bulian, G, Souto-Iglesias, A, Delorme, L, and Botia-Vera, E (2010). "Smoothed Particle Hydrodynamics (SPH) Simulation of a Tuned Liquid Damper (TLD) with Angular Motion," *Journal of Hydraulic Research*, 48, 28-39.

Bouscasse, B, Colagrossi, A, Souto-Iglesias, A, and Cercos-Pita, JL (2014a). "Mechanical Energy Dissipation Induced by Sloshing And Wave Breaking in a Fully Coupled Angular Motion System I. Theoretical Formulation and Numerical Investigation," *Physics of Fluids*, 26(3), 033103.

Bouscasse, B, Colagrossi, A, Souto-Iglesias, A, and Cercos-Pita, JL (2014b). "Mechanical Energy Dissipation Induced by Sloshing and Wave Breaking in a Fully Coupled Angular Motion System. II. Experimental Investigation," *Physics of Fluids*, 26(3), 033104.

Cummins, SJS, and Rudman, M (1999). "An SPH Projection Method," *Journal of Computational Physics*, 152(2), 584–607.

Delorme, L, Colagrossi, A, Souto-Iglesias, A, Zamora-Rodríguez, R, and Botía-Vera, E (2009). "A Set of Canonical Problems in Sloshing, Part I: Pressure Field in Forced Roll-comparison between Experimental Results and SPH," *Ocean Engineering*, 36(2), 168–178.

Housner, GW (1963). "The Dynamic Behavior of Water Tanks. *Bulletin of the Seismological Society of America*," 53(2), 381–387.

Hwang, SC, Park, JC, Gotoh, H, Kayyer, A, and Kang, KJ (2016). "Numerical Simulation of Sloshing Flows with Elastic Baffles by Using a Particle-based Fluid-structure Interaction Analysis Method". *Ocean Engineering*, 118, 227-241.

Kondo, M, and Koshizuka, S (2011). "Improvement of Stability in Moving Particle Semi-implicit Method," *Int. J. Numer. Methods Fluids* 65, 638–654.

Koshizuka, S, and Oka, Y (1996). "Moving Particle Semi-Implicit Method for Fragmantation of Incompressible Fluid," *Nuclear Science and Engineering*, 123, 421–434.

Lee, BH, Park, JC, Kim, MH, and Hwang, SC (2011). "Moving Particle Simulation for Mitigation of Sloshing Impact Loads Using Surface Floaters", *CMES*, vol. 75, no. 2, 89-112.

Lee, BH, Park, JC, Kim, MH, and Hwang, SC (2011). "Step-by-step Improvement of MPS Method in Simulating Violent Free-Surface Motions and Impact-loads," *Computer methods in applied mechanics and engineering*, 200(9), 1113-1125.

Souto-Iglesias, A, Botia-Vera, E, Martín, A, and Pérez-Arribas, F (2011). "A Set of Canonical Problems in Sloshing. Part 0: Experimental Setup and Data Processing," *Ocean Engineering*, 38(16), 1823–1830.

Souto-Iglesias, A, Bulian, G, and Botia-Vera, E (2015). "A Set of Canonical Problems in Sloshing. Part 2: Influence of Tank Width on Impact Pressure Statistics in Regular Forced Angular Motion," *Ocean Engineering*, 105, 136–159.

Tanaka, M, and Masunaga, T (2010). "Stabilization and Smoothing of Pressure in MPS Method by Quasi-Compressibility," *Journal of Computational Physics*, 229(11), 4279-4290.

Tang, ZY, Zhang, YX, and Wan, DC (2014). "Overlapping MPS Method for 2D Free Surface Flow," *International Society of Offshore and Polar Engineers*, Busan, 3, 411-419.

Van Daalen, EFG, and Kleefsman, K (2001). "Anti-Roll Tank Simulations with a Volume of Fluid (VOF) based Navier-Stokes Solver," *EPRINTS-BOOK-TITLE*.

Vera, EB, Iglesias, AS, Bulian, G, and Lobovský, L (2010). "Three SPH Novel Benchmark Test Cases for Free Surface Flows," *Proceedings of the 5th ERCOFTAC SPHERIC Workshop on SPH Applications*, 2010.

Verhaegen, JHG and Van Wyngarden, L (1965). "Non-linear Oscillations of Fluid in a Container," *Journal of Fluid Mechanics*, 22(4), 737–751.

Zhang, YX, and Wan, DC (2012) "Numerical Simulation of Liquid Sloshing in Low-filling Tank by MPS," *Chin. J. Hydrodyn*, 27, 100–107.

Zhang, YX, and Wan, DC (2011). "Application of Improved MPS Method in Sloshing Problem," *Proc. of the 23rd Chinese Symposium on Hydrodynamics,* Xi'an, China, 156-162.